A&A 379, 185–198 (2001)
DOI: 10.1051/0004-6361:20011312

Astronomy & Astrophysics

Spectroscopy of TT Arietis in "positive superhumps" state⋆

V. Stanishev⋆⋆, Z. Kraicheva⋆⋆, and V. Genkov⋆⋆

Institute of Astronomy, Bulgarian Academy of Sciences, 72 Tsarigradsko Shouse Blvd., 1784 Sofia, Bulgaria

Received 11 April 2001 / Accepted 8 August 2001

Abstract. An analysis of spectral and photometric observations of the novalike TT Ari obtained in the interval 1999–2001 is presented. The photometry in November 1999 shows "positive superhumps" with a period of $0\overset{\mathrm{d}}{.}14815$ and full amplitude 0.13–0.14 mag. The emission lines equivalent widths are also modulated with the "positive superhumps" period, as its value in the interval from August 2000 to January 2001 is $0\overset{\mathrm{d}}{.}148815$. The analysis shows that the flux in the emission lines vary in anti-phase with the continuum. It is found that Hα asymmetry is modulated with the expected precessional period of $1\overset{\mathrm{d}}{.}81715$ supporting the precession accretion disc model for the "positive superhumps" observed in TT Ari. An expansion of the TT Ari accretion disc due to a mass transfer rate reduction is proposed as a possible mechanism for the appearance of the "positive superhumps". The Hα profile shows a weak, blue-shifted absorption, whose strength is modulated with the orbital period of the system. The Hα Doppler tomogram reveals the presence of an asymmetric source of emission in the accretion disc. Eclipse of this emission source by the outflowing wind is the most likely explanation of the phase dependent Hα P-cygni profile. The He I λ6678 tomogram shows a strong asymmetric emission source located at the back side of the disc. The asymmetric emission sources in Hα and He I λ6678 tomograms are thus located on the opposite sides of the system mass center. The emission of the secondary is detected in He I λ6678 Doppler tomogram, which allows us to secure the absolute phasing of the radial velocities. We derive a new orbital ephemeris of TT Ari by analysis of all availible high state radial velocities.

Key words. accretion, accretion discs – stars: individual: TT Ari – novae, cataclysmic variables – X-ray: stars

1. Introduction

The novalike (NL) TT Ari is the only superhumper known to replace its "negative superhumps" ($P \simeq 0\overset{\mathrm{d}}{.}1330$) with "positive" ones ($P_{\mathrm{sh}} \simeq 0\overset{\mathrm{d}}{.}1492$). The replacement was discovered by Skillman et al. (1998), who predicted an apsidal precession period of $1\overset{\mathrm{d}}{.}76$ and absorption lines asymmetry modulated with this period. Kraicheva et al. (1999a) showed that the period change happened between 1996 and 1997, and that in 1998 the star was still in the "positive superhumps" regime. The authors also found that some quantities related to the flickering changed as generally the flickering activity decreased by a factor of 2 during the "positive superhumps" regime.

Spectral observations in "negative superhump" regime (Cowley et al. 1975; Vojkhanskaya 1983; Thorstensen et al. 1985, hereafter TSH; Shafter et al. 1985; Hutchings & Cote 1985; Hutchings et al. 1986) have shown that TT Ari has single-peaked emission lines and is a low-inclined system with $i \simeq 20{-}30°$, mass ratio $q \simeq 0.4$ and $P_{\mathrm{orb}} = 0\overset{\mathrm{d}}{.}13755114$. The most essential result from the spectroscopy is that the phasing of the emission line radial velocities (RVs) depends on the brightness level as the low state RVs are ∼180° out of phase with the high state ones. The most reasonable explanation of this seems to be that emission from at least two sources is observed and their relative contribution changes with the brightness of the star.

In this paper we present our spectral and photometric observations of TT Ari obtained from 1999 to 2001. The goal is to investigate the behaviour of the star in the "positive superhumps" state.

2. Observations and data reduction

The spectral observations of TT Ari were obtained at Rozhen National Astronomical Observatory from January 2000 to January 2001. The Coudé spectrograph of the 2.0-m telescope in combination with a Photometrics 1024^2 CCD camera and 632 lines mm^{-1} grating was used. This resulted in ∼0.35 Å spectral resolution (as measured

Send offprint requests to: V. Stanishev,
e-mail: vall@astro.bas.bg

⋆ Based on observations obtained at Rozhen National Astronomical Observatory, Bulgaria.

⋆⋆ e-mail: zk@astro.bas.bg (Z.K.), nao@mail.orbitel.bg (V.G.)

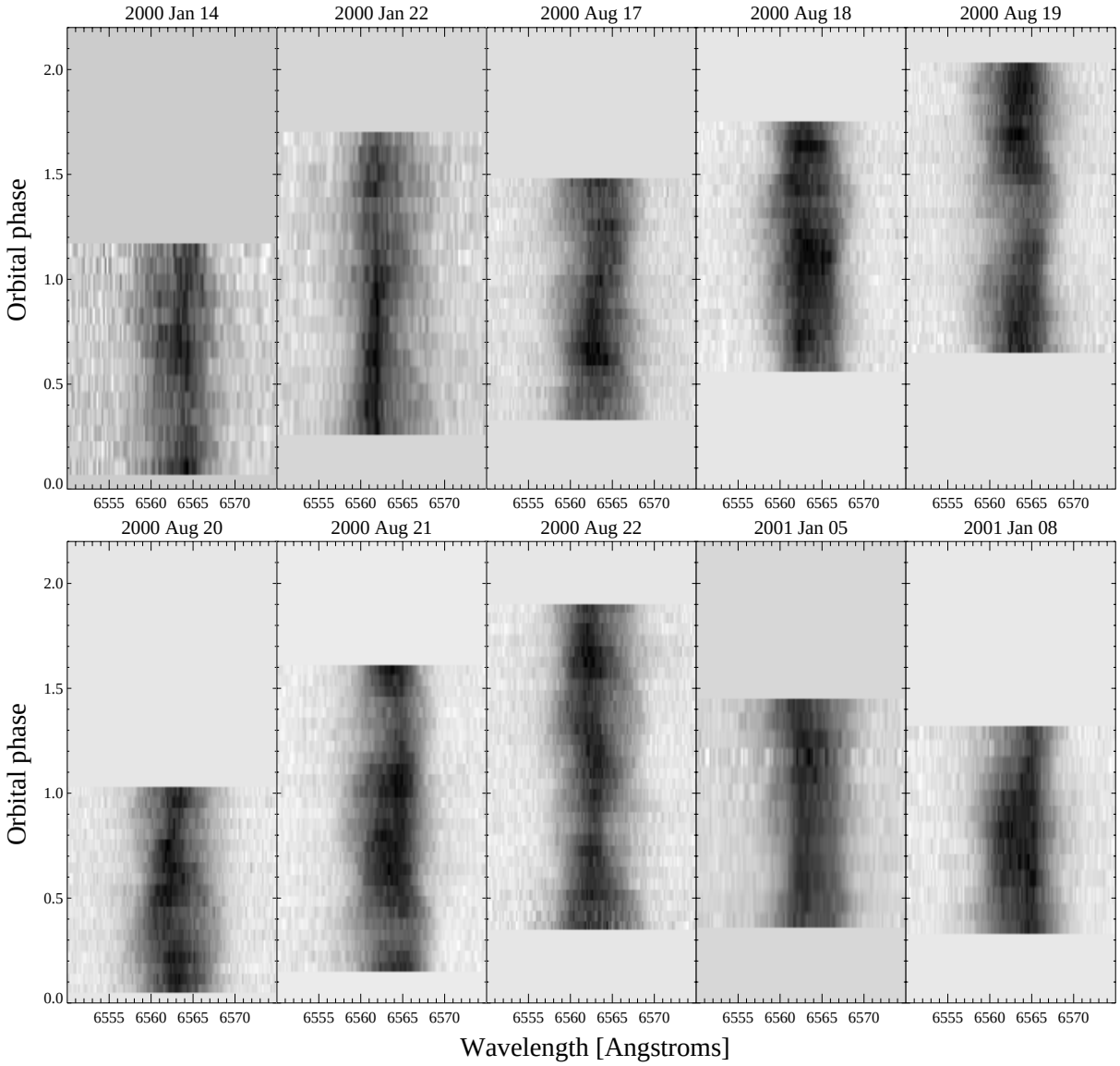

Fig. 1. Trailed grey-scale representation of the Hα profiles from the series covering at least one orbital cycle. The spectra are displayed in the order of obtaining, but on the vertical axis are shown the orbital phases calculated with Eq. (1). The resulting small gaps from the comparison spectra measurements are filled by interpolation between phases.

from the full-width at half maximum (*FWHM*) of the comparison spectra lines) and a wavelength coverage of ∼200 Å. The exposure times varied from 10 to 20 min depending on the seeing and the detector sensitivity in the observed spectral region. The data were reduced in a standard way with bias and night sky spectrum subtraction, flat field corrections, and extraction of the 1D spectra from the 2D images by the optimal method of Horne (1986). ThAr and FeAr arc lamp spectra were used for wavelength calibration. When long series were obtained, comparison spectra were regularly taken during the night. The rms scatter around the second-order polynomial fits to the arc lines was always <0.015 Å. Some details of the spectral observations are given in Table 1. Since we were unable to correct for the slit loses, flux standards were not observed and the spectra were only normalised to the continuum. The trailed Hα profiles from the long series, covering at least one orbital cycle are shown in Fig. 1.

Before or after the spectral observations, measurements in the standard *UBV* system were obtained, which show that TT Ari was in high state with $V \simeq 10.9-11.0$. In addition, several long B runs were obtained in November 1999, and September and October 2000. A log of the photometric observation is given in Table 2. Figure 2 shows the long-term light curve of TT Ari (Kraicheva et al. 1999a; this paper) with the positions of our long spectral series and data used by TSH to determine the orbital ephemeris marked.

Table 1. Spectral observations of TT Ari.

Date	HJD start 2 450 000+	S/N (mean)	Number of spectra	Exp. [min]
2000 Jan. 14	1558.182	12	14	15[a]
2000 Jan. 22	1566.186	15	18	15[a]
2000 Aug. 15	1772.532	24	3	20[b]
2000 Aug. 16	1773.586	23	2	20[b]
2000 Aug. 17	1774.445	26	22	10[b]
2000 Aug. 18	1775.440	25	23	10[b]
2000 Aug. 19	1776.415	25	26	10[b]
2000 Aug. 20	1777.433	26	19	10[b]
2000 Aug. 21	1778.410	29	28	10[b]
2000 Aug. 22	1779.399	27	30	10[b]
2000 Sep. 13	1801.451	25	13	15[c]
2000 Sep. 14	1802.493	25	9	20[d]
2000 Sep. 15	1803.517	25	10	15[c]
2000 Nov. 16	1865.477	44	1	15[e]
2000 Nov. 17	1866.267	43	2	15[e]
...	1866.294	40	1	15[b]
2000 Nov. 18	1867.495	29	1	20[b]
...	1867.515	31	1	20[e]
2000 Dec. 08	1887.325	32	1	20[b]
...	1887.352	50	1	20[c]
...	1887.373	42	1	20[d]
2001 Jan. 05	1915.303	31	13	15[b]
2001 Jan. 07	1917.175	40	12	20[e]
...	1917.365	32	7	15[c]
2001 Jan. 08	1918.188	31	13	15[b]

[a] Hα; [b] Hα + He I λ6678; [c] Hβ; [d] Hγ; [e] He II λ4686.

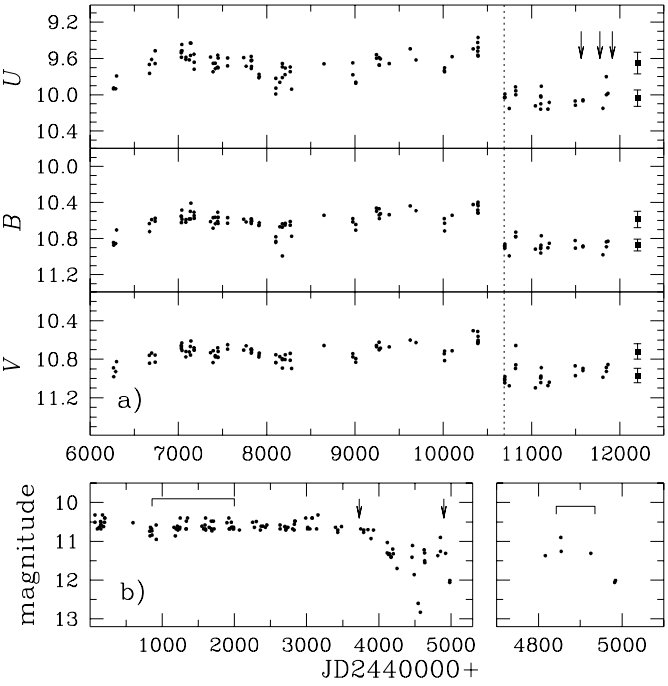

Fig. 2. a) UBV long-term light curve of TT Ari. The dashed vertical line marks the supposed time of period change. The arrows show the moments when long spectral series were obtained. The error bars ($\pm1\sigma$) show the mean magnitudes of the star before and after the period change. **b)** Part of TT Ari long-term light curve showing when the spectral data used by TSH to determine the orbital ephemeris were obtained.

Table 2. Flickering characteristics.

Date	Filter	Duration [hours]	γ	τ [s]	Standard deviation
1999 Nov. 12	B	6.5	1.97	134	0.025
1999 Nov. 13	B	7.2	1.75	141	0.021
1999 Nov. 14	B	6.8	1.68	162	0.020
2000 Sep. 20	B	3.5	1.63	208	0.028
2000 Oct. 29	B	2.2	1.89	150	0.021
2000 Oct. 30	B	2.5	1.69	203	0.023
2000 Oct. 31	B	2.8	2.00	185	0.027

3. Results

3.1. Photometry

The periodogram analysis (Fig. 3; Scargle 1982) of the B band series reveals that in 1999 and 2000 the star was still in a "positive superhumps" state. The 2000 runs are short and sparsely distributed, and a precise value of the "positive superhumps" period could not be determined. The strongest peak in the 1999 data periodogram corresponds to a period of $\sim 0\overset{\mathrm{d}}{.}14815$, but the accuracy of this value is limited by the short baseline of the observations. The semi-amplitude of the modulations in both data sets is $\sim$0.06$-$0.07 mag (as determined by a sinusoidal fitting) and is consistent with the values found in 1997 and 1998 observations (Skillman et al. 1998; Kraicheva et al. 1999a). We also derived the flickering characteristics: the power spectrum slope γ, the characteristic time scale τ and the standard deviation in the curves after the positive superhumps have been subtracted (see for details Kraicheva et al. 1999b). It is found that these characteristics (Table 2) are consistent with those determined by Kraicheva et al. (1999a) for the TT Ari "positive superhumps" regime.

3.2. Mean emission lines profiles

In the left panel of Fig. 4 are shown the mean Hβ, Hγ and C III/N III λ4645 + He II λ4686 emission lines profiles, and an expanded view of the continuum around Hα. All emission lines are narrow ($FWHM \simeq$ 330–400 km s^{-1}) and single-peaked suggesting a rather low-inclined system. Hβ and Hγ emission lines are superimposed over broad absorptions, which can be traced up to $\sim\pm$2000 km s^{-1}. These absorptions are believed to originate in the optically thick parts of the accretion disc and are most probably additionally broadened by the pressure effect. We measured their equivalent widths (EW) (negative in our convention) by fitting Gaussians to the parts of the mean profiles which are not affected by the emission core. For both Hβ and Hγ we obtained $\simeq -2.75$ Å.

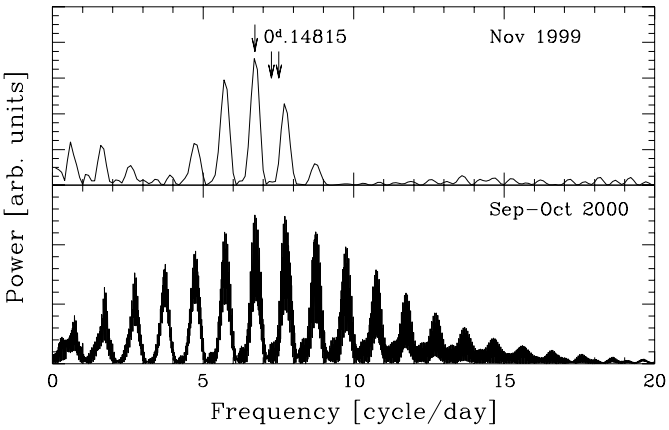

Fig. 3. Periodograms of the B band series obtained in 1999 and 2000. The arrows mark the "positive superhumps", orbital and "negative superhumps" periods.

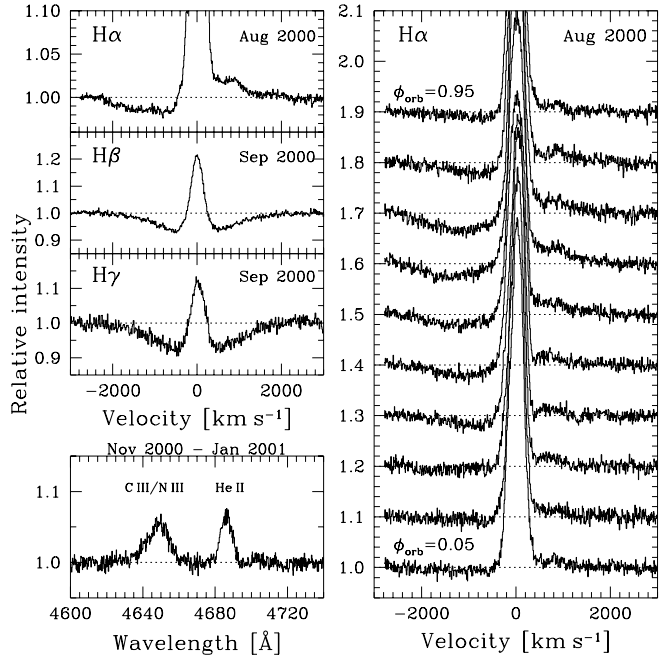

Fig. 4. *Left panel*: from top to bottom: expanded view of the continuum around Hα, mean profiles of Hβ, Hγ and He II λ4686 + C III/N III λ4645. *Right panel*: the continuum around Hα averaged in 10 phase bins. Phases are calculated according to the TSH ephemeris.

The shape of the continuum around Hα suggests a broad, weak and blue-shifted absorption component. Similar features are commonly observed in the UV resonance emission lines of low inclination cataclysmic variables (CVs) and indicate mass outflow from the system (Mauche & Raymont 1997). Recently such absorptions were also discovered in the optical spectra of some novalikes (BZ Cam – Patterson et al. 1996; Ringwald & Naylor 1998; V751 Cyg – Patterson et al. 2001). The inspection of the individual spectra immediately reveals the tendency of the absorptions to appear predominantly in orbital phases of 0.4–0.9 (TSH). The absorption component is not seen in all spectra in these phases but it is rather like short-lived (of the order of the exposure time) absorption events, similar to those observed in V751 Cyg. The right panel of Fig. 4 shows August 2000 spectra averaged in 10 phase bins. The vertical scale is expanded in order to see more clearly the blue-shifted absorption. It is seen that the absorption is phase dependent reaching a maximum $EW \simeq -1$ Å near phase 0.75. Phase-dependent P-cygni profiles of TT Ari UV emission lines have already been reported by Robinson & Cordova (1994) and our data shows similar behaviour of Hα. While in the UV this is considered as a common feature of the CVs (Drew & Verbunt 1988; Woods et al. 1992) only V751 Cyg is known to show this phenomenon in the optical (Patterson et al. 2001).

It is interesting to note that TSH found a systematic difference in the RV amplitudes of the different Balmer emission lines of TT Ari. The authors showed that this is due to the systematically higher RVs of the lower lines near the minima of the folded curves and pointed out that a blue-shifted absorption, stronger in the lower Balmer lines, could account for this effect. We do see this absorption in Hα, but the Hβ and Hγ spectra are not enough to say if the blue-shifted absorption is present in these lines too.

Besides the blue-shifted absorption, there is an extended emission tail on the red side of Hα. This emission is seen during the whole orbital cycle and seems to be phase-dependent too: it is stronger when the absorption is deeper. Similar red tails in Hα have been reported for three other NLs (MV Lyr – Skillman et al. 1995; BZ Cam and V751 Cyg – Patterson et al. 1996, 2001) as in V751 Cyg the strength of the emission tail also correlates with the absorption.

The analysis that follows was performed after the continuum around the emission lines was fitted and the spectra were normalized to the fits. For Hβ and Hγ this was done by fitting Gaussians to the parts of the profiles which are not affected by the emission core, while the local continuum around Hα and He I λ6678 was approximated by a straight line.

3.3. Equivalent widths

The periodogram of Hα EWs in August 2000 spectra (Fig. 5 lowest panel) reveals a strong modulation with a period of $\sim 0\overset{\mathrm{d}}{.}1488$, i.e. close to the "positive superhumps" period in the photometric light curves. If the period of this modulation does not change significantly during the interval of the observations and if we assume that the EWs of all the Balmer lines vary in phase, the period can be more precisely determined by applying the TSH technique used to refine the TT Ari orbital ephemeris. Briefly, if the data are considered as consisting of several segments, for the correct value of the period the EWs in all segments have to vary in phase. In practice, the data are folded over a fine grid of periods and the phase of the modulation in each data segment is determined by a sinusoidal

Table 3. The mean *EW*s and semi-amplitudes of the modulations as determined by sinusoidal fits to the data shown in Fig. 5.

line	Mean *EW* [Å]	Semi-amplitude [Å]
Aug.–Sep. 2000		
Hα	5.46 (0.04)	0.76 (0.05)
Hβ	2.05 (0.03)	0.42 (0.04)
Hγ	1.51 (0.04)	0.43 (0.07)
He I 6678	0.69 (0.01)	0.17 (0.01)
Nov. 2000–Jan. 2001		
Hα	5.90 (0.09)	0.58 (0.13)
Hβ	1.85 (0.21)[1]	...
He I 6678	0.74 (0.02)	0.21 (0.04)
He II 4686	0.52 (0.17)[1]	...
N III/C III 4645	0.83 (0.17)[1]	...

[1] Mean value and standard deviation.

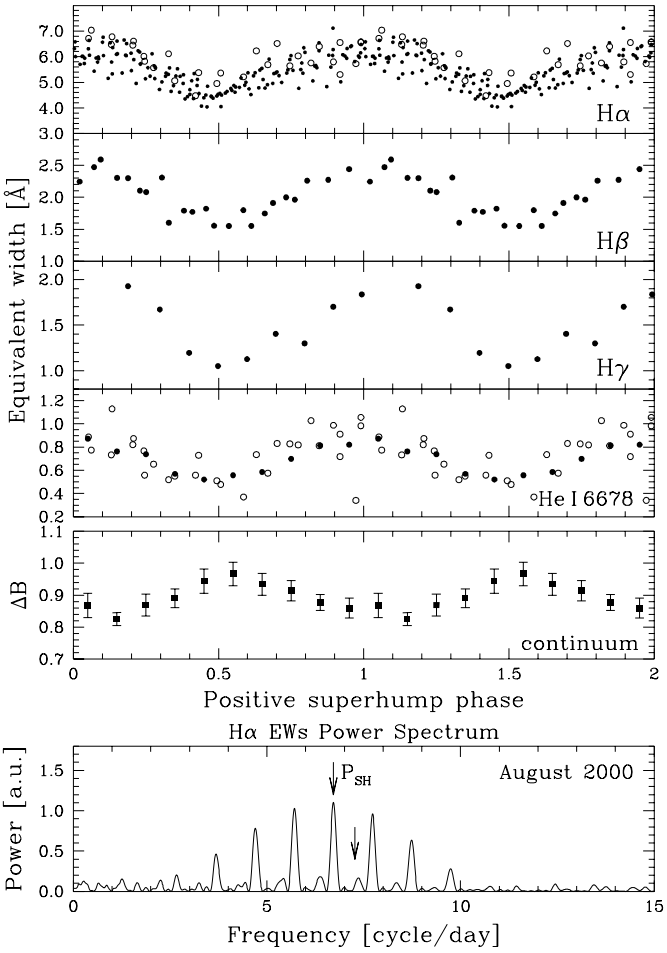

Fig. 5. Hα, Hβ, Hγ and He I λ6678 *EW*s, and the continuum B light curve folded with the $0\overset{\mathrm{d}}{.}148815$ period. The B series taken after September 2000 are averaged in 10 phase bins and the error bars are $\pm1\sigma$. For Hα and He I λ6678 the filled circles show August 2000 data and the open ones November 2000–January 2001 data. In the lowest panel is shown the periodogram of the Hα *EW*s in August 2000. The arrows mark the $0\overset{\mathrm{d}}{.}148815$ and orbital periods.

fitting. The best period is that for which the rms of the phases around the mean is least. The data in January 2000 do not show well-defined *EW* modulation and were not analysed. Thus, the *EW*s were divided into three groups, Hα – August 2000, Hβ+Hγ – September 2000 and Hα – November 2000–January 2001 and we searched for the period between $0\overset{\mathrm{d}}{.}147$ and $0\overset{\mathrm{d}}{.}15$. The analysis shows that with the period of $0\overset{\mathrm{d}}{.}148815$ the *EW*s in the three segments vary in phase. The *EW*s folded with this period are shown in Fig. 5. Since the He I λ6678 line is weak, its *EW*s in August 2000 were measured from the spectra averaged in 10 phase bins. It is seen that the He I λ6678 *EW*s are in phase with those of the Balmer lines. The *EW*s in the three segments were fitted separately and the fits parameters are given in Table 3. The corresponding errors come from the fitting program. For some emission lines the semi-amplitude is not given because the data are not sufficient to follow the modulation. In these cases the error of the mean value is $\pm1\sigma$. The period derived above is based on data obtained over an interval of six months and covering many cycles, and hence it is more accurate than that determined from the photometry (Sect. 3.1). Because of this, in the following analysis we have accepted that the "positive superhumps" period in 2000 is $0\overset{\mathrm{d}}{.}148815$. Moreover, it is known that most of the permanent "positive superhumpers" show long-term period variations (Patterson 1999) and we have no guarantee that the period in 2000 coincides with that in 1999.

It can be expected that the continuum light and the emission lines *EW*s are modulated with the same period. Folding of the 2000 season B runs with the $0\overset{\mathrm{d}}{.}148815$ period shows that this is indeed the case. The folded light curve averaged in 10 phase bins is shown in Fig. 5. It is seen that the *EW*s and B continuum are almost exactly anti-phased. This behaviour is expected if the *EW* modulation is due to variations only in the continuum or if the continuum and line fluxes vary in phase but the continuum is more strongly modulated. If this is the case, however, the relative amplitude of the *EW* modulation will be equal or less than that of the continuum. Our data show the opposite – the relative semi-amplitudes of the *EW* modulations are higher than that of the B continuum, which is $\Delta F_{\mathrm{c}}/\bar{F}_{\mathrm{c}} \simeq 0.065$. Therefore, the emission lines fluxes have to vary in anti-phase with the continuum. We note that the relative amplitude of the *EW* modulations increases toward the higher lines. It is assumed here that the continuum around Hα/He I λ6678 is modulated by the same degree as the B continuum.

The data given in Table 3 suggest that the Hα and He I λ6678 *EW*s in November 2000–January 2001 are ∼8% higher. Our data are not spectrophotometric and the absolute line fluxes are uncertain. We can however use UBV photometry to constrain the continuum flux at

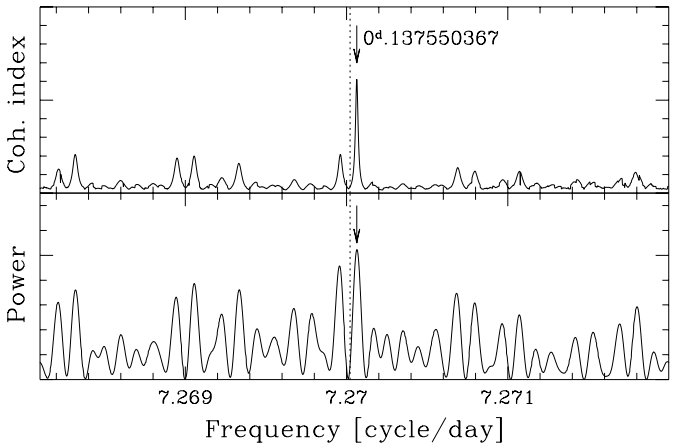

Fig. 6. The phase coherence index and Lomb-Scargle periodogram in the vicinity of the orbital period. Dashed vertical line shows the TSH orbital period of TT Ari.

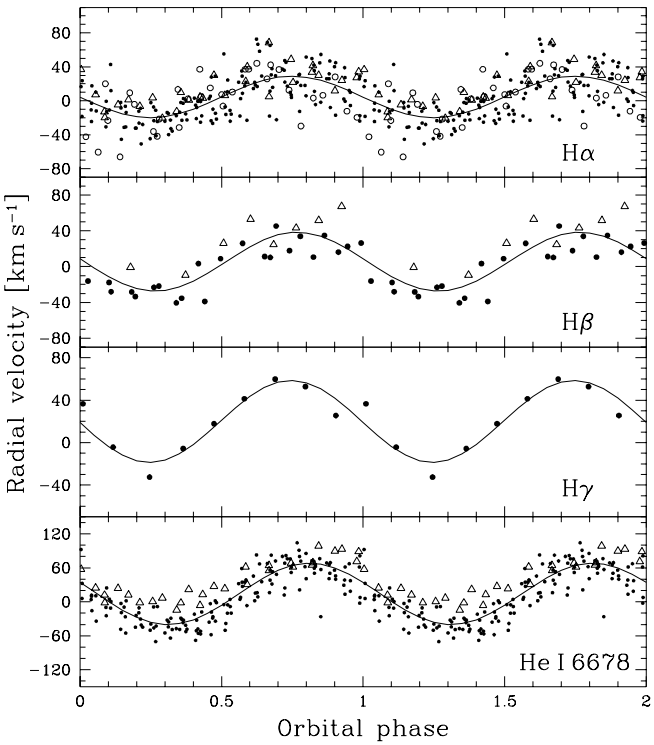

Fig. 7. The line wings *RV*s of the TT Ari emission lines folded with Eq. (1). The best sinusoidal fits are also shown and the corresponding parameters are given in Table 4. Open circles, filled circles and triangles show January 2000, August 2000 and January 2001 data, respectively.

different wavelengths. This gives a flat Balmer decrement, suggesting an emission from optically thick gas, and $F(\mathrm{He\,II}\,\lambda4686)/F(\mathrm{H}\beta) \simeq 0.3$, a value typical for NLs (Vojkhanskaya 1987). It is also interesting to note that the ratio of the C III/N III $\lambda4645$ blend and He II $\lambda4686$ fluxes seems to be state dependent: greater than unity in high state (Cowley et al. 1975; this work) and less than unity in intermediate state (Hutchings & Cote 1985).

3.4. Radial velocities

The emission lines *RV*s were measured by the double-Gaussian technique of Schneider & Young (1980) as refined by Shafter (1983). Gaussians with $\sigma = 1$ Å were used and the optimal separation was determined from the diagnostic diagrams (not shown) obtained with the known orbital period of TT Ari. For Hα, Hβ and He I $\lambda6678$ the optimal separation was the point just before the relative scatter around the folded curve sine fit starts to increase. As we have only nine Hγ spectra, in this case the optimal separation was a compromise between the *RV*s amplitude and the relative scatter. With the separations used, 730, 620, 430 and 360 km s^{-1} for Hα, Hβ, Hγ and He I $\lambda6678$, respectively, we measure the *RV*s of the line wings, which are thought to arise close to the white dwarf (WD) and are more or less expected to give an estimation of its true dynamic motion. In most *CV*s the presence of asymmetric sources of emission, such as the bright spot, affects the *RV*s and they do not follow the WD motion. The trailed Hα profiles (Fig. 1) and single-trailed Hα profile (Fig. 10) of TT Ari suggest the presence of a high velocity *s*-wave in the line wings. Figure 10 also shows that He I $\lambda6678$ emission line is dominated by two anti-phased *s*-waves. Since we actually measure the line wings *RV*s, these *s*-waves can affect significantly both amplitude and phase of the *RV* curve. Thus, the *RV* amplitudes we obtained are probably strongly biased and cannot be used for system parameters determination.

The *RV*s folded with TSH ephemeris show that the inferior conjunction is not at zero phase as it should be, but is at $\phi \simeq 0.6$ (that of He I $\lambda6678$ *RV*s comes later at $\phi \simeq 0.67$). As our data are ∼22 yr away from the initial epoch of TSH ephemeris, such a displacement could be generally caused by secular period changes or/and by using a slightly incorrect ephemeris. To accumulate almost half a cycle O–C residuals for 22 yr requires a very high rate of period change. This is physically unreasonable and we will not discuss it anymore. Thus, we reanalysed all published high state *RV*s in order to derive a new ephemeris of TT Ari. Figure 6 shows the phase coherence index (TSH) and the periodogram in the vicinity of the expected frequency. The phase coherence index was calculated as the *RV*s were divided in eight data segments. Both periodogram analyses indicate a slightly shorter period of $0\overset{\mathrm{d}}{.}137550367$. To check the consistency we have folded the *RV*s in each segment with this period and found that the phase in one of the segments, that obtained in JD 2444843–935, significantly deviates from the others. The inspection of the TT Ari long-term light curve (Fig. 2b) shows that this data set was obtained between the only known low state of TT Ari (∼16 mag) and the preceding intermediate state. The observations were obtained in a moment when the star was bright but still ∼0.5 mag fainter than its usual high state magnitude. TT Ari has been known to show a state dependent

Table 4. Sine fit parameters to the emission lines *RV*s.

line	reference	state	γ [km s^{-1}]	K [km s^{-1}]	ϕ_0^a	σ [km s^{-1}]	ϕ_0^b	ϕ_0^c
(1)	(2)	(3)	(4)	(5)	(6)	(7)	(8)	(9)
Hα	this work	high	5.7 (1.3)	25.8 (1.9)	−0.013 (0.012)	19.0	−0.107	0.593
Hβ	···	high	5.5 (3.3)	32.9 (4.5)	0.016 (0.023)	18.2	−0.077	0.620
Hγ	···	high	20.0 (4.0)	38.6 (5.8)	−0.005 (0.023)	12.2	−0.097	0.602
He I 6678	···	high	14.0 (1.7)	54.2 (2.5)	0.061 (0.007)	23.0	−0.031	0.671
Hδ+	Cowley et al. (1975)	high	4.5 (3.6)	65.0 (5.3)	−0.023 (0.012)	27.5	−0.004	0.007
Hγ	TSH (I)	high	33.8 (5.0)	56.7 (7.0)	0.010 (0.020)	29.4	0.004	−0.053
Hβ	TSH (II)	high (?)	13.5 (2.2)	24.9 (3.0)	0.147 (0.020)	20.6	0.128	0.036
Hβ	TSH	intermediate	47.5 (6.5)	28.6 (8.6)	0.380 (0.054)	28.5	0.366	0.283
Hβ+	Hutchings et al. (1986)^d	high	7.0 (3.0)	28.0 (4.0)	−0.017 (0.043)	17.0	−0.026	−0.096
Hβ+	Hutchings & Cote (1985)	intermediate	−1.9 (3.0)	37.3 (4.4)	0.275 (0.018)	15.3	0.254	0.119
Hα	Shafter et al. (1985)^d	low	11.0 (4.0)	93.0 (6.0)	0.608 (0.007)	–	0.583	0.473

^{a} Equation (1); ^{b} Eq. (3); ^{c} TSH ephemeris; ^{d} values taken from the articles.

phase of its *RV*s (Hutchings et al. 1986) and therefore a slightly different phase in these data might be expected. Since the observations in question are a significant part of the whole data set used by TSH and since the phase coherence index is sensitive to such phase variations, it is possible that the obtained period is slightly incorrect. Note also that the *RV*s amplitude of Hβ in this data set is by a factor of 2 lower than that in the other TSH high state data (22 and 54 km s^{-1}), which probably indicates that the star is not in the same state. In addition, there are small phase offsets still remaining in the TSH data relative to their ephemeris. The authors discussed them as a result of phase variations due to changes in the relative contribution of the different emission sources. We notice that these phase offsets could be produced if the phase is different in one of the data sets only. Of course there is no doubt that TSH ephemeris is the best in the sense of describing the particular data set analysed, but it can still be biased as discussed above.

We thus repeated the analysis excluding the data discussed above and obtained the following ephemeris which describes the times of superior conjunction:

$$T_0 = 2\,451\,800.39563(385) + 0.137550367(35)E. \quad (1)$$

The *RV*s (including those obtained in intermediate and low state) were folded with this ephemeris and fitted with the equation $V_r = \gamma - K\sin[2\pi(\phi - \phi_0)]$ (Hutchings et al. (1986) and Shafter et al. (1985) have only given the moments of *RV*s extrema and inferior conjunction, respectively, and we converted them into phases). The resulting parameters are given in Cols. 4–7 of Table 4 and our observations phased with Eq. (1) are shown in Fig. 7. It is seen that except for the TSH data discussed above (labeled as TSH (II) in Table 4) and to some extent the He I λ6678 *RV*s, the high state *RV*s are well represented by Eq. (1). The phase offset of TSH (II) data is +0.147 and seems to follow the "magnitude–*RV*s phase" relation established by Hutchings & Cote (1985). As we will see in Sect. 3.7, our *RV*s probably do not follow the WD motion and hence the ephemeris derived above is also biased. However, we have used it in the following analysis because it puts the superior conjunction of our data at zero phase. Besides, we note that the two periods differ by only 0.067 s and which of them is used has no effect on the results.

3.5. Hα asymmetry

A closer inspection of the spectra reveals that apart from the Hα asymmetry variations on orbital time scale there are night-to-night changes; during a given night the blue or red part of the line remains stronger. To demonstrate this we measured the wavelengths which separate the emission lines in two parts of equal flux. The corresponding *RV*s for August 2000 and January 2001 data are shown in the upper panel of Fig. 8. The idea that the distorted velocity field in a precessing, eccentric accretion disc has to produce emission lines whose asymmetry is modulated with the precession period was introduced by Hessman et al. (1992). Patterson et al. (1993) observed this effect in the absorption lines of the helium-reach CV AM CVn and supposed that emission lines of the *CV*s with precessing, eccentric discs should have similar behaviour.

If the accretion disc precesses in inertial coordinate system with period $P_{\rm prec}$, then the "positive superhumps" period $P_{\rm sh}$ is given by:

$$\frac{1}{P_{\rm sh}} = \frac{1}{P_{\rm orb}} - \frac{1}{P_{\rm prec}}. \quad (2)$$

With $P_{\rm orb} = 0\overset{\rm d}{.}137550367$ and $P_{\rm sh} = 0\overset{\rm d}{.}148815$, the expected precession period is $1\overset{\rm d}{.}81715$. The data are sparsely distributed and are not very suitable for a direct periodicity search. Because of this we only checked if they could

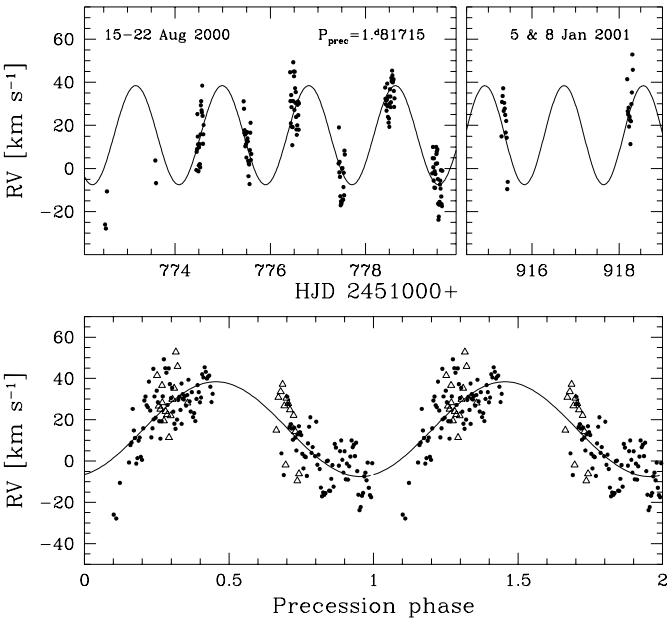

Fig. 8. *Upper panel*: the *RV*s corresponding to the wavelengths separating Hα in two parts of equal flux. The best fit with the expected precession period of 1^d.81715 is also shown. *Lower panel*: the same data folded with the precession period. The August 2000 and January 2001 data are shown with filled circles and triangles, respectively.

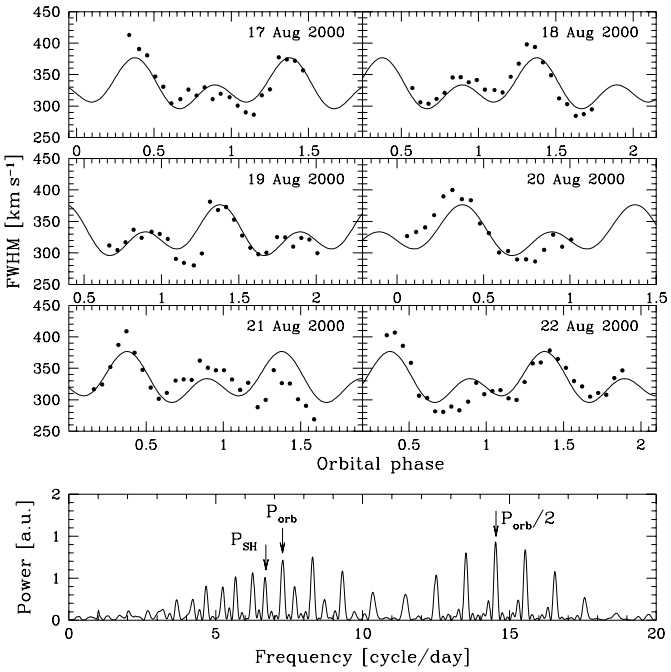

Fig. 9. *Upper panels*: the Hα *FWHM*s and the best fit obtained with the three detected periods: "positive superhumps" period, orbital period and its first harmonic. *Lower panel*: the periodogram of the Hα *FWHM*s in August 2000. The detected periods are marked with arrows.

be fitted with the precession period. The best fit is shown in Fig. 8 and it describes the data fairly well. The lower panel of Fig. 8 shows the folded curve. The filled circles and the triangles are August 2000 and January 2001 data, respectively. This result suggests that the "positive superhumps" in TT Ari are generated by a precessing, eccentric accretion disc and that the precession period was stable from August 2000 to January 2001. The attempt to fit the whole data set (including the spectra taken in January 2000) failed as the January 2000 data are not fitted. This is not unexpected because the photometric studies have shown that the TT Ari "positive superhumps" period is not very stable and dances around a mean value of $\sim$0^d.149, which is most probably due to variations of the precession period.

3.6. FWHM of Hα emission line

The *FWHM* of Hα was measured after the spectra were convolved with a Gaussian with σ = 0.5 Å and interpolation between the spectral points. The periodogram of the *FWHM*s of Hα in August 2000 spectra is shown in the lower panel of Fig. 9. In spite of the complexity introduced by the strong 1-day aliases, three peaks are identified. They correspond to the "positive superhumps" period, orbital period and its first harmonic. The sinusoidal fit with these periods is shown with the solid line in the upper panels of Fig. 9. To explain the *FWHM* modulation with the "positive superhumps" period one has to assume that Hα is composed by at least two components whose fluxes vary with this period, but have different fractional amplitudes (or one of them remains constant). Modulations of the *FWHM* of an emission line with the first harmonic of the orbital period can be introduced by a *s*-wave moving twice per orbital cycle across the line. A comparison between the trailed spectra and Fig. 9 shows that Hα is widest at the phases when the *s*-wave in the line wings is maximally blue or red shifted (0.35 and 0.85). This phasing strongly suggests that the *s*-wave is responsible for the observed modulation. The most puzzling observation is the modulation with the orbital period. As it is not detected in the *EW*s, its appearance in the *FWHM* is somewhat unexpected and the corresponding peak could be the first sub-harmonic of the $P_{\rm orb}/2$ period. Figure 9 shows, however, that the maxima of the Hα *FWHM* around phase 0.35 are generally greater than those around phase 0.85. This asymmetry is also seen in the single-trailed spectrum (upper left panel of Fig. 10) and probably this is the cause for the appearance of the peak in the periodogram. If two parts of Hα are modulated with $P_{\rm orb}$ but vary in anti-phase and have nearly equal fluxes, then the *EW*s will remain constant while the *FWHM* will be modulated. Although this seems to be a reasonable explanation, Hα is not well resolved by components and the two sources could not be unambiguously identified.

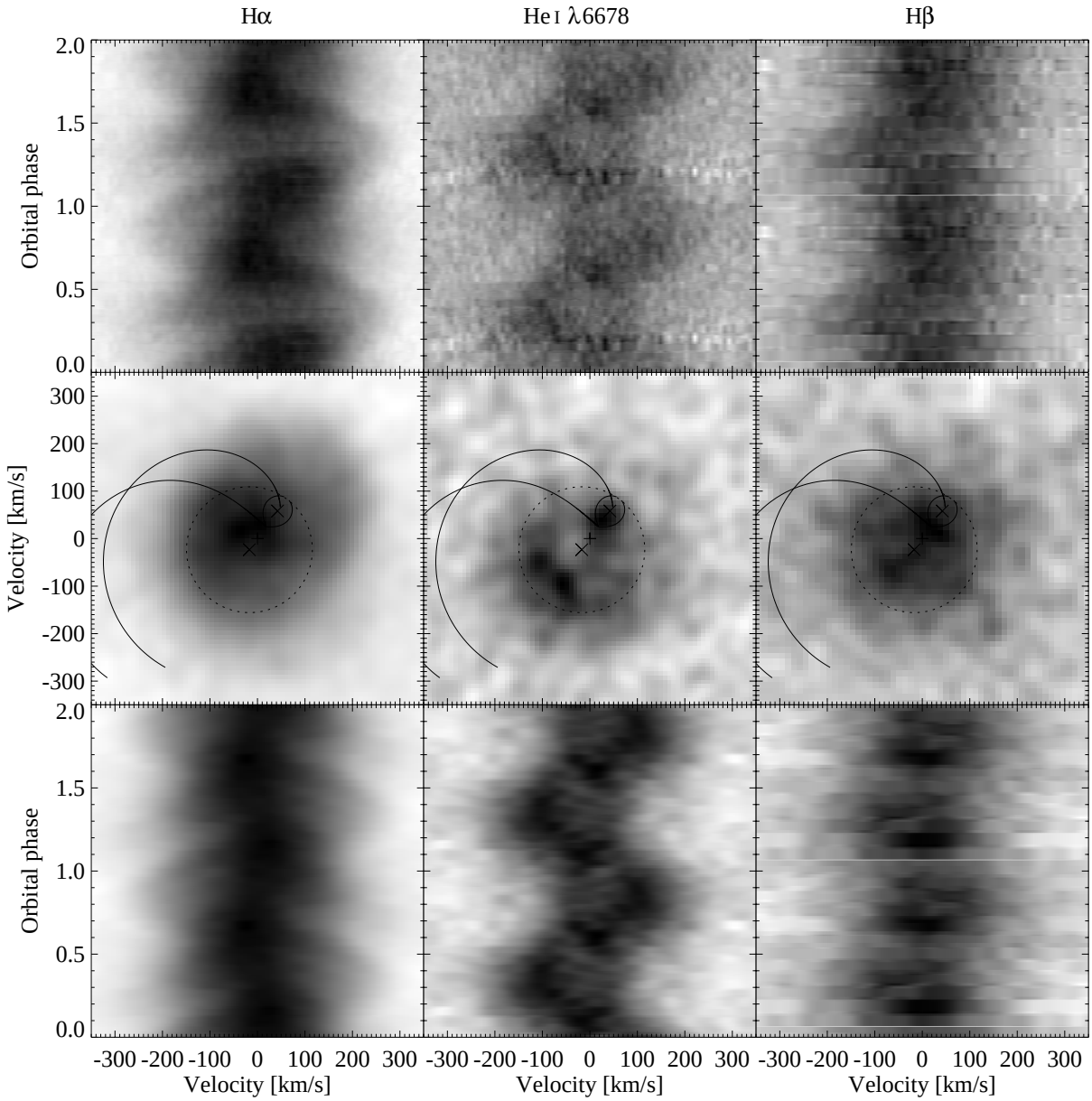

Fig. 10. From top to bottom: single-trailed grey-scale representation of TT Ari Hα, He I λ6678 and Hβ spectra, the calculated Doppler tomograms and back-projected from them spectra. The trailed spectra are repeated for clarity. On the tomograms are also overplotted the centers of the two stars, the Roche lobe of the secondary, and the accretion stream with its true velocities and with the Keplerian velocities in the disc along the stream path. The dashed circle represents the Keplerian velocity in the disc at the distance from the WD equal to its Roche lobe radius. All these components are rotated by 0.1 cycles clockwise (see text for details).

3.7. Doppler tomography

The Doppler tomograms of Hα, Hβ and He I λ6678 emission lines were calculated from the spectra taken from August 2000 to January 2001. We used the Fourier-filtered back-projection method (Marsh & Horne 1988; Horne 1991). In Fig. 10 from top to bottom are shown the trailed spectra, the tomograms and the calculated from them trailed spectra. For velocities greater than $\sim$300 km s^{-1} the tomograms consist of nothing but noise and because of this they are shown up to $\sim$350 km s^{-1} only.

The tomograms of TT Ari have to be interpreted cautiously because some of the basic assumptions of Doppler tomography are obviously violated. First, the line flux is not constant but varies with the "positive superhumps" period and second, due to the accretion disc precession the emission lines asymmetry is modulated with the precessional period. Since the superhumps period is $\sim$8.2% longer than the orbital the extrema of the emission line flux come $\sim 0.6 P_{\rm orb}$ later each night. In this case observations on consecutive nights, as most of ours are, can ensure a correct reconstruction of the mean flux.

The second problem is more serious and an incomplete precession cycle coverage could introduce suspicious structures in tomograms. Observations covering many orbits and well distributed over the precession cycle can help in obtaining artifact-free tomograms, but the eccentric disc shape could not be reconstructed. The eccentric shape of the disc will be axially smoothed and the resulting tomograms are expected to be axisymmetric.

The comparison between the observed and the back-projected from the calculated tomograms trailed spectra shows that the main features (the *s*-waves) are fairly well reconstructed. Most of the He I λ6678 emission comes from two sites located on the opposite sides of system center of masses. That at $(V_x, V_y) \simeq (+30, +50)$ km s^{-1} has an amplitude of $\sim$55 km s^{-1} and is confined in a narrow velocity interval. Emission from the secondary is often observed in *CV*s and the properties of the spot suggest that it most probably arises there by reprocessing the hard radiation of the WD and inner hot parts of the accretion disc. The spot is displaced from $+V_y$ axis and to put the secondary inner hemisphere over the spot requires $i \simeq 15°$ and a rotation clockwise by $\sim$0.1 cycles (we use $q = 0.4$). The different system elements are plotted in Fig. 10 assuming these values. Using high resolution Hα spectra in the low state, Shafter et al. (1985) measured velocity amplitude of the secondary to be $\sim$90 km s^{-1}. This value is $\sim$60% higher than ours and we have no explanation of this discrepancy. The second emission site in the He I λ6678 tomogram has an arc/ring shape, sub-Keplerian velocities and is extended $\sim$180° along the azimuth. Moving in antiphase with the secondary, it could be associated with the back side of the disc. It is worth mentioning that emission from the hot spot is not seen in He I λ6678.

A significant part of the emission in Hα comes from gas with sub-Keplerian velocities. There is also a weak circular emission which can be seen up to $\sim$280–300 km s^{-1}. In the asymmetric image (Fig. 11) this emission component is not seen showing that it is centered on the WD and thus most probably arises in the accretion disc. The presence of the high velocity *s*-wave in the line wings results in an asymmetric tomogram elongated along the line connecting the two stars. This is better seen in the asymmetric Hα image where an enhanced emission from the $(+V_x, +V_y)$ quadrant is clearly detected. There are also two other asymmetric sources of emission. One of them can be associated with the hot spot if it is assumed that the accretion disc fills the WD Roche lobe. The other one has low velocity and is centered at $(V_x, V_y) \simeq (-10, +30)$.

To examine which parts of Hα and He I λ6678 emission lines are involved in the emission lines flux variations we calculated Doppler maps from the spectra covering 0.4 of the "positive superhumps" cycle around the *EW*s maxima and minima. Since the "positive superhumps" and orbital periods are different, the spectra in the two sets cover well the orbital cycle. It turned out that Hα asymmetry introduced strong artifacts in the tomograms because not all orbital and precessional phases are equally covered. To avoid this we corrected the Hα profiles in the following way. The mean profile for each run was calculated and the spectra were divided by it. Then each spectrum was multiplied by the mean profile determined from all spectra. Figure 12 shows the resulting tomograms as the intensity scale is the same for the minimum and maximum *EW*s images. We have also computed the Hα tomogram (not shown) from all corrected spectra. It is identical with that calculated from the row spectra suggesting that artifacts are probably not introduced by the applied correction. Moreover, the Hα tomograms shown in Fig. 12 are very similar to the original one (Fig. 10).

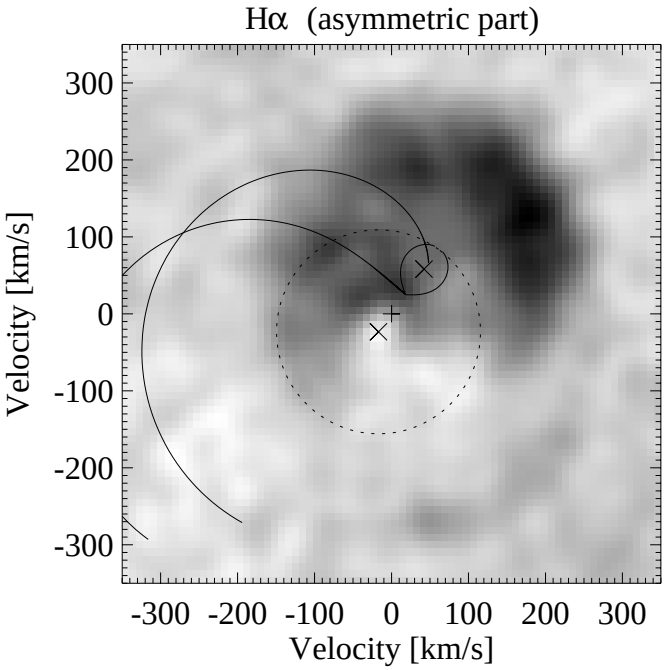

Fig. 11. The asymmetric part of the Hα tomogram calculated as the symmetric part of the image centered on the WD has been subtracted.

The He I λ6678 tomograms show that the emission from the secondary remains relatively constant and that the other emission source is responsible for the He I λ6678 flux variations. The most apparent difference between the Hα tomograms in minimum and maximum *EW*s is that in the latter one the low velocity emission at $(V_x, V_y) \simeq (-10, +30)$ and the hot spot are both stronger. Besides, the hot spot emission seems to be biased toward higher velocities. The shape of the high velocity asymmetric emission also changes, being more extended toward low velocities in the *EW*s maximum. Thus, the analysis shows that all asymmetric sources of emission are involved in Hα flux modulations.

The most apparent feature of the Hβ tomogram is the emission from the expected position of the secondary and in this aspect it is similar to that of He I λ6678. The remaining part of the Hβ emission has a sub-Keplerian velocity similarly to Hα. Note however that the Hβ tomogram is calculated from small number of spectra and

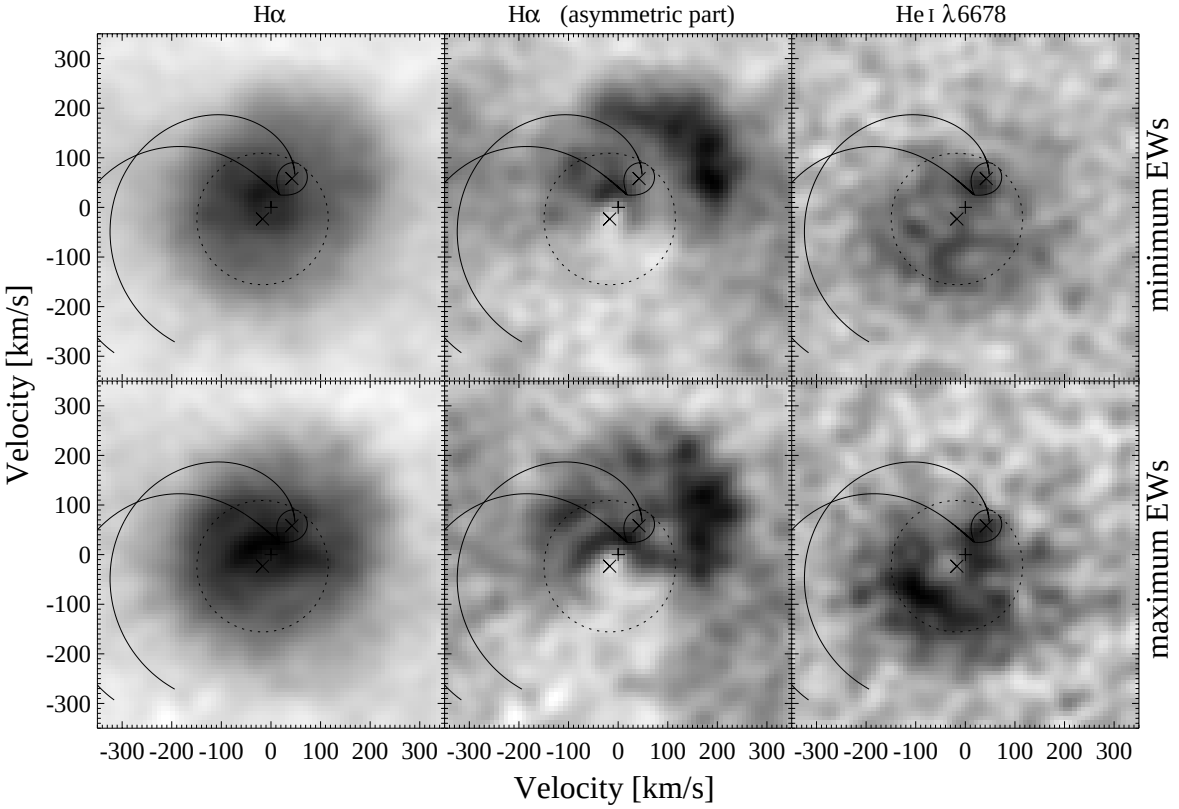

Fig. 12. Doppler tomograms of Hα and He I λ6678 emission lines calculated from the spectra taken around the *EW*s minima (upper row) and maxima (lower row). The asymmetric Hα images are also shown.

probably suffers from artifacts. Because of this we will not discuss it anymore.

4. Discussion

"Positive superhumps" observed in SU UMa stars during superoutbursts and in some NLs are believed to be a result of slow precessing under the gravitational perturbation of the secondary eccentric accretion discs. Although our results support this model for TT Ari superhumps, there are still some problems. It has been shown that non-axisymmetric discs in *CV*s are formed under the action of the 3:1 resonance, i.e. when the Keplerian period at the outer disc edge is three times shorter than the orbital (Lubow 1991; Whitehurst 1988; Murray 1998). The 3:1 resonance can be reached only in systems with $q \leq 0.3$. The mass ratio of TT Ari determined from the spectroscopy is $\simeq$0.4 (Cowley et al. 1975) and the same value is obtained by applying Patterson's (1998) $\epsilon(q)$ relation for the "positive superhumps". Thus, TT Ari is not expected to show "positive superhumps". Recent numerical simulations of Murray et al. (2000) have shown, however, that a sudden reduction of the mass transfer rate by a factor of 2 results in an expansion of the accretion disc and it almost fills the WD Roche lobe. If such an expansion takes place in a system with $q \simeq 0.33$, the outer disc edge could eventually reach the 3:1 resonance and Murray et al. (2000) supposed that this mechanism could operate in the VY Scl novalikes, which show low states. The long-term UBV light curve of TT Ari is shown in Fig. 2a as the dashed vertical line roughly marks the epoch when the system started displaying "positive superhumps". It is seen that after this moment the system is fainter by $\sim$0.3 mag in B, a value consistent with a reduction of the mass transfer rate of approximately two. If accretion discs in systems with $q \simeq 0.4$ also respond to mass transfer rate reductions with an expansion, then it can be expected that the accretion disc in TT Ari is large and almost fills the WD Roche lobe. The estimations show that if Keplerian frequency at $r_{\rm d} \simeq 0.95 R_{\rm RL}$ is reduced by $\sim$10$-$15%, the outer disc edge will be in 3:1 resonance with the orbital period. The mechanism that can force the matter to rotate slower is not clear; however the tidal influence of the secondary could do the job.

TT Ari is a non-eclipsing binary and it is difficult to obtain the system parameters accurately. In low-inclined systems such as TT Ari the *RV*s amplitude is expected to be rather low and less than the low-to-intermediate resolution of the spectra generally used in *CV*s studies. Besides, the *RV*s of NLs are known to be strongly biased by additional s-waves and do not represent the true dynamic motion of the WD. Thus, the possibility that the mass ratio of TT Ari is not accurately determined cannot be ruled out and it could actually be $\sim$0.33. In this

case the reduction of Keplerian frequency at the outer disc edge is not needed to reach the 3:1 resonance and only the mechanism proposed by Murray et al. (2000) could be responsible for the observed "positive superhumps".

There are two types of "positive superhumps" in SU UMa dwarf novae: "normal" and "late". Both of them have nearly equal periods but the modulations are anti-phased. "Normal superhumps" are observed during the superoutbursts maxima when the disc is large, hot and optically thick, while the "late" ones appear during the very late stages of superoutburst when the system becomes fainter by roughly 1–1.5 mag. The "normal superhumps" most likely originate in the elongated outer part of the disc, which is additionally heated by the extra tidal stress from the secondary. They reach a maximum then the elongated part of the disc points to the secondary. On the other hand "late superhumps" are produced by a modulation of the hot spot emission and are observed when the accretion disc luminosity fades and the spot can be seen. The "late superhumps" reach their maxima when the elongated part of the disc points away from the secondary, i.e. when the gas in the stream hits the more dense part of the disc thus giving rise to the hot spot contribution (Hessman et al. 1992). The presence of broad underlying absorptions in the higher Balmer lines of TT Ari shows that the accretion disc is in a hot and optically thick state and therefore "normal" superhumps are expected. However, Rolfe et al. (2000) found that the superhumps in the eclipsing nova-like V348 Pup are consistent with a hot spot origin, which suggests that the "late superhumps" can be observed in some high mass transfer systems.

To first-order approximation both the accretion disc and hot spot luminosities in a steady accretor are proportional to the mass transfer rate. Therefore, their ratio is expected to be nearly constant for all systems in a steady accretion regime. However, steady accretion discs in NLs are optically thick and the combined action of limb darkening and foreshortening is expected to significantly reduce the contribution of the disc to the total luminosity of a high-inclined NL. This allows the hot spot to become more visible and indeed, in a study of six eclipsing NLs by the eclipse mapping method (Horne 1985), Rutten et al. (1992) found hot spots contributing up to 13% of the total system light. Thus, a modulation of the hot spot emission can produce superhumps. At lower inclinations the accretion disc becomes very bright and the contribution of the spot should be highly reduced (in addition, if a simple model in which the hot spot light is emitted from a perpendicular to the orbital plane area is assumed, in low inclination systems the spot will be foreshortened and will contribute even less). Therefore, it is questionable if the hot spot in a low inclination system, such as TT Ari, can produce superhumps with a full amplitude of $\sim$0.13−0.14 mag. A modulation of the spot luminosity can however produce weak superhumps and an evidence for this is found in the numerical simulations. The pseudo-light curves extracted from the simulations of Murray (1996) show strong "normal superhumps" plus weak secondary humps arising from the hot spot and placed in the minima of the main wave. Kraicheva et al. (1999a) pointed out the presence of such secondary, low amplitude humps in some of the minima of the TT Ari light curves. We see this feature in some of our B runs too. Therefore, the weak secondary humps seen in the light curves of TT Ari could be "late superhumps".

The identification of the emission of the secondary in He I λ6678 Doppler tomogram provides us with the opportunity to secure the absolute phasing of TT Ari RVs, at least at the time of our observations. Figure 10 shows that the tomogram is rotated by $\sim$0.1 cycles clockwise, which implies that the absolute superior conjunction is at phase +0.1. Starting from Eq. (1) we obtained the following ephemeris:

$$T_0 = 2\,451\,800.27077 + 0.13755057E \quad (3)$$

which describes the high state RVs and places the superior conjunction of our RVs at phase −0.1. The sinusoidal fitting of the RVs folded with this equation gives the ϕ_0's listed in Col. 8 of Table 4 (the errors coincide with those in Col. 7). For a comparison we have also listed in Col. 9 the ϕ_0's respective to TSH ephemeris. It is seen that our ephemerides describe all high state RVs better, if of course TSH (II) data set is not considered. In almost all NLs the conjunction of the emission line source does not coincide with the true dynamic conjunction. Thus, which of our two ephemerides is closer to the real one depends on some assumptions concerning the phasing of the old high state RVs (about which we of course have no information). If the offset is *negative* as in our data, then Eq. (1) will be closer to the true ephemeris. The vast majority of NLs (and CVs as a whole) show however *positive* offsets. If this is the case in TT Ari (or have no offset) then Eq. (3) is better. Apart from the phase offset of TSH (II) RVs, another potential problem of both our ephemerides is that the superior conjunction of the low state RVs is not exactly at phase 0.5. We do not consider this so worrisome because the emission lines in TT Ari low state are not pure emission from the secondary (Shafter et al. 1985) and hence can also be biased.

The Doppler tomograms of TT Ari Hα and He I λ6678 emission lines (Fig. 10) are quite different and this is rather surprising since both lines are low excitation ones. The s-waves corresponding to the main asymmetric sources of emission in Hα and He I λ6678 are anti-phased and therefore their sources are on the opposite sides of the system center of masses. Thus, the question is why the s-wave seen in He I λ6678 does not appear in Hα and the opposite. To our knowledge there are no other CVs showing similar behaviour and in the absence of theoretical models we will only outline the possible models that could explain He I λ6678 and Hα tomograms separately.

The asymmetric emission in He I λ6678 tomogram has low, sub-Keplerian velocities. If the accretion disc in TT Ari fills the WD Roche lobe and its outer edge rotates with sub-Keplerian velocity, as was already discussed, then this arc-shaped emission could be associated

with the outer disc rim. Hoard et al. (1998) developed a model in which a thick, asymmetric bulge, formed far along the disc rim by the stream/disc impact is responsible for the peculiarities observed in SW Sex novalikes (SW Sex phenomenon was recently reviewed by Hellier 2000). The bulge is illuminated by the hard radiation of the inner disc and the WD, and an enhanced emission from it is observed (a similar model is also accepted in the modeling of the super soft X-ray sources by Meyer-Hofmeister et al. 1997). The other models of SW Sex stars (Hellier 1998; Horne 1999) could not be ruled out; however note that they predict emission from sites with somewhat higher velocities than observed in TT Ari. Another possibility is TT Ari to be an intermediate polar. The Doppler tomograms of the intermediate polar RX J0558+53 (Still et al. 1998; Harlaftis & Horne 1999) are almost identical with the He I λ6678 tomogram of TT Ari. Harlaftis & Horne (1999) supposed that the acr-shaped emission component could be a result of the impact between the part of the stream overflowing the disc (Lubow 1989) and the magnetosphere of the WD. The shocked, emitting gas moves with the rotational velocity of the magnetosphere and gives the relatively low-velocity arc-shaped structure in the Doppler image.

The most interesting feature in the Hα tomogram is its asymmetric shape, a result from the high velocity *s*-wave which is permanently present in the spectra (Fig. 1). The only system component moving with the velocity of the asymmetric emission is the accretion disc. Thus, this emission component most probably arises there. The mechanism that can produce it however is rather uncertain. A possible explanation might be the spiral shocks recently detected during the outbursts of some dwarf novae (Steeghs 2000 and references therein). Both the simulations and observations show however that spirals are formed always in pairs and while the asymmetric emission observed in TT Ari Hα tomogram coincides with one of them, the absence of the other cannot be easily explained. Note also that the asymmetric emission could account for the observed phase-dependent P-cygni profile of Hα. According to our new ephemerides the blue-shifted absorption is strongest at phases $\sim$0.5–0.6. If the wind in TT Ari is strongly collimated, then the outflowing gas will be projected over the asymmetric structure only around these phases, as observed.

The analysis shows that the spectral behaviour of TT Ari in the "positive superhumps" regime is very complex. Doppler tomograms of Hα and He I λ6678 lines reveal several asymmetric emission sources. The *s*-waves corresponding to these asymmetric emission components are really presented in the data (Fig. 10) and could be explained in several ways. Since Hα and He I λ6678 images are very different, it is not easy to find a single model which is able to explain both of them. Such a modeling is out of the scope of this paper and we have only outlined the models which could explain the Hα and He I λ6678 Doppler tomograms separately. Probably the mechanism responsible for the peculiarities observed in TT Ari is a complex combination between some of the models mentioned above. We note however that the situation is most likely highly complicated by the presence of a precessing, eccentric accretion disc. Certainly, observations of more emission lines (including higher excitation ones such as He II λ4686) with good S/N, and spectral and time resolution are needed in order to clarify the situation.

Acknowledgements. The work was partially supported by NFSR under project No. 715/97.

References

Cowley, A., Crampton, D., Hutchings, B., & Marlborough 1975, ApJ, 195, 413
Drew, J., & Verbunt, F. 1988, MNRAS, 234, 341
Harlaftis, E., & Horne, K. 1999, MNRAS, 305, 437
Hellier, C. 2000, NewAR, 44, 131
Hellier, C. 1998, PASP, 110, 420
Hessman, F. V., Mantel, K.-H., Barwig, H., & Schoembs, R. 1992, A&A, 263, 147
Hoard, D., Szkody, P., Still, M., Smith, R. C., & Buckley, D. A. H. 1998, MNRAS, 294, 689
Horne, K. 1985, MNRAS, 213, 129
Horne, K. 1986, PASP, 98, 600
Horne, K. 1991, in Fundamental Properties of Cataclysmic Variable Stars, Pros. 12th N. Am. Workshop on Cataclysmic Variables and Low Mass X-ray Binaries, ed. A. Shafter (San Diego State University, San Diego), 23
Horne, K. 1999, ASP Conf. Ser. 157, ed. C. Hellier, & K. Mukai, 349
Hutchings, J., & Cote, T. 1985, PASP, 97, 847
Hutchings, J., Thomas, B., & Link, R. 1986, PASP, 98, 507
Kraicheva, Z., Stanishev, V., Genkov, V., & Iliev, L. 1999a, A&A, 351, 607
Kraicheva, Z., Stanishev, V., & Genkov, V. 1999b, A&AS, 134, 263
Lubow, S. H. 1989, ApJ, 340, 1064
Lubow, S. H. 1991, ApJ, 381, 259
Marsh, T., & Horne, K. 1988, MNRAS, 235, 269
Mauche, C. W., & Raymond, J. C. 1997, in Cosmic Winds and the Heloisphere, ed. J. R. Jokipii, C. P. Sonett, & M. S. Giampapa (Tucson: University of Arizona Press), 111
Meyer-Hofmeister, E., Schandl, S., & Meyer, F. 1997, A&A, 231, 245
Murray, J. R. 1996, MNRAS, 279, 402
Murray, J. R. 1998, MNRAS, 297, 323
Murray, J. R., Warner, B., & Wickramasinghe, D. T. 2000, MNRAS, 315, 707
Patterson, J. 1998, PASP, 110, 1132
Patterson, J. 1999, in Disk Instabilities in Close Binary Systems, 25 Years of the Disk-Instability Model. Proc. of the Disk-Instability Workshop held on 27–30 October, 1998, Kyoto, Japan, Front. Sci. Ser. 26, ed. S. Mineshige, & J. C. Wheeler (Universal Academy Press, Inc.), 61
Patterson, J., Halpern, J., & Shambrook, A. 1993, ApJ, 419, 803
Patterson, J., Patino, R., Thorstensen J., et al. 1996, AJ, 111, 2422
Patterson, J., Thorstensen, J., Fried, R., et al. 2001, PASP, 113, 72
Ringwald, F., & Naylor, T. 1998, AJ, 115, 286
Robinson, C., & Cordova, F. 1994, ASP Conf. Ser., 56, 146

Rolfe, D. J., Haswell, C. A., & Patterson, J. 2000, MNRAS, 317, 759
Rutten, R. G. M., van Paradijs, J., & Tinbergen, J. 1992, A&A, 260, 213
Scargle, J. D. 1982, ApJ, 263, 835
Schneider, D. P., & Young, P. 1980, ApJ, 238, 946
Shafter, A. W. 1983, ApJ, 267, 222
Shafter, A. W., Szkody, P., Liebert, J., et al. 1985, ApJ, 290, 707
Skillman, D., Patterson, J., & Thorstensen, J. 1995, PASP, 107, 545
Skillman, D., Harvey, D., Patterson, J., et al. 1998, ApJ, 503, L67
Steeghs, D. 2000 [astro-ph/0012353]
Steeghs, D., Horne, K., Marsh, T. R., & Donati, J. F. 1996, MNRAS, 281, 626
Still, M. D., Duck, S. R., & Marsh, T. R. 1998, MNRAS, 299, 759
Thorstensen, J., Smak, J., & Hessman, F. 1985, PASP, 97, 437 (TSH)
Voikhanskaya, N. F. 1983, Astron. Zh., 60, 1155
Voikhanskaya, N. F. 1987, Astron. Zh. Lett., 13, 397
Whitehurst, R. 1988, MNRAS, 232, 35
Woods, J., Verbunt, F., Collier Cameron, A., Drew, J., & Piters, A. 1992, MNRAS, 255, 237